Synthesis of N-doped and non-doped partially oxidised graphene membranes supported over ceramic materials

J Mater Sci

Synthesis of N-doped and non-doped partially oxidised graphene membranes supported over ceramic materials

A. Giménez-Pérez[1], S. K. Bikkarolla[2], J. Benson[2], C. Bengoa[1], F. Stüber[1], A. Fortuny[3], A. Fabregat[1], J. Font[1,*], and P. Papakonstantinou[2,*]

[1] Departament d'Enginyeria Química, Universitat Rovira i Virgili, Av. Països Catalans 26, 43007 Tarragona, Spain
[2] School of Engineering, Engineering Research Institute, Ulster University, Newtownabbey BT37 0QB, UK
[3] Departament d'Enginyeria Química, Universitat Politècnica de Catalunya, EUPVG, Av. Víctor Balaguer, s/n, 08800 Vilanova i la Geltrú, Spain

Received: 9 March 2016
Accepted: 17 May 2016

ABSTRACT

Graphene has a great potential to substitute other amorphous carbon materials and has been widely used in many water and wastewater treatments such as purification or photocatalytic processes. Graphene powder with different degrees of oxidation was synthesised and subsequently used to prepare supported membranes. Ceramic porous materials were chosen as membrane support due to the robustness and long life required in a likely application. Ultrathin membranes (7–9 μm) were successfully prepared through vacuum filtration of highly oxidised graphene or reduced graphene oxide solutions (1 mg ml^{-1}). The influence of depositing different amounts of membrane precursor was extensively studied (0.003–0.037 mg cm^{-2}); above 0.037 mg cm^{-2}, drying-related shrinkage problems are detected. Moreover, the ceramic support pore size (SPS) (0.008–0.08 μm) shows little impact in terms of the overall membrane flux resistance, and the deposited graphene layer usually governs the membrane permeation. Finally, long-term filtration experiments were also performed for weeks without substantial variation of the membrane structure or permeation (≤2 %), which is demanded in most conventional water treatments. Overall, the addition of partially oxidised graphene to conventional ceramic membranes greatly decreases their electrical resistivity ($\sim 2.8 \times 10^{-5}$ Ω m), opening up the possibility of being employed for many environmental purposes.

Address correspondence to E-mail: jose.font@urv.cat; p.papakonstantinou@ulster.ac.uk

DOI 10.1007/s10853-016-0075-5

Published online: 13 June 2016

Introduction

Since its first report in 2004, graphene has become one of the main attractions of the scientific world due to its outstanding electrical, optical and mechanical properties [1]. Monolayer graphene shows Young's modulus of 1 TPa and fracture strength of 130 ± 10 GPa, being considered the world's strongest material [2]. Some studies have estimated its electrical resistance as only 20.16 Ω/sq [3] and optical transparency around 97.7 % [4]. Initially, single-layer graphene nanosheets were prepared by mechanical exfoliation of bulk graphite, also known as the "scotch tape" method [5]. However, the exfoliation of the highly ordered pyrolytic graphite allows for the preparation of only small areas between nanometres and micrometres in lateral dimension [6]. A different approach to synthesise graphene, epitaxial chemical vapour deposition (CVD), is commonly used for applications that require small areas of high-quality graphene [7–10]. On the contrary, CVD shows a lack of controllability when transferring graphene films between different substrates, and it is not the best technique to synthesise homogeneous large-area size [11].

An absolutely different method is the chemical reduction of exfoliated graphite oxide [12]; unlike the other techniques, this one allows for the synthesis of graphene in large scale and reasonable cost [13]. In 1958, Hummers and Offeman [14] developed a rapid and relatively safe method to synthesise the highly oxidised graphene oxide (GO) from graphite. This technique introduced a new way to prepare GO using $KMnO_4$ and $NaNO_3$ in concentrated H_2SO_4, which is suitable for large-scale production [15], and is commonly used to prepare large GO films [16–19]. GO oxygen groups can be removed by different physical [20] or chemical methods [21]. In this study, GO was reduced by the solvothermal method [22].

GO is a promising material to fabricate membranes because of its hydrophilicity, excellent strength, large surface area, low flux resistance and relevant permeation [23]. In addition, the intrinsic 3D heterogeneous structure of GO films may also help to improve the selectivity [24, 25], since open gaps between the stacked platelets are approximately of 1 nm width [26], and thus, these gaps can act as nanopores for molecular transport [27]. GO membranes can be useful in many applications, such as filters for water treatment, catalysis, electrical devices, or molecular sieving processes [28–30]. The fabrication of these GO films involves different techniques including Langmuir–Blodgett assembly [31], vacuum filtration [24], molecular templates [19], spin-coating [13, 32] and spray coating. On the contrary, reduced graphene oxide (RGO), yet showing hydrophobic properties, provides higher electrical conductivity than GO. For these reasons, RGO membranes can be applied in water processes where minimising the electrical resistance is needed [33]. Great efforts have been taken in depositing uniform films onto substrates, which has been considered as a major hurdle; this study is focused on the vacuum filtration technique, which has been successfully applied to prepare graphene films with different oxidation degrees. A notable advantage is the possibility of controlling perfectly the membrane thickness [24, 29].

Graphene membranes are reported as freestanding films [34–39] or supported ones [40, 41]. However, most water treatment processes are subjected to high pressures, so that membranes must be robust enough to operate for long periods, therefore supported membranes are preferred. Ceramic materials have been reported as membrane support, because they possess many important advantages such as high thermal and chemical stability, pressure resistance, long lifetime, and catalytic properties arising from their intrinsic nature [42, 43]. The chemical stability is highly significant especially for membrane modification or preparation processes. Hence, ceramic porous elements offer the possibility to be used as support for the graphene layer becoming a composite membrane.

This study deals with the preparation of GO and nitrogenated RGO (GO and NrGO) membranes supported over ceramic porous materials. To the best of our knowledge, there are no previous studies involving the synthesis of GO or NrGO membrane supported over ceramics (ZrO_2–TiO_2), focusing on the influence of the graphene oxidising degree, amount of membrane precursor employed for the preparation or the pore size of the ceramic support. These membranes could enhance many environmental processes where other adsorbent and conductive materials are currently being used [44, 45], such as activated carbon filters [46]. Potential applications include photocatalytic or biological processes. Photocatalysis is a clean technology, which uses semiconductor-based nanomaterials such as carbon-based films (TiO_2/activated carbon) [47] to separate

and remediate contaminated organic wastewater [48]. However, decorating titania photocatalyst with GO is of particular interest due to GO's ability to increase the photocatalytic activity of TiO_2 [49]. On the other hand, graphene-based membranes can be employed to intensify the biodegradation of recalcitrant pollutants present in wastewater, which cannot be efficiently removed by conventional methods. Some of these processes are limited by the electron transfer in redox systems [46]; at this point, both GO and specially NrGO provide better properties as electron mediator than other ones, such as activated carbon, which have been widely employed over recent decades [50]. Moreover, GO offers a 3D sponge structure favouring the microbial growth and presents excellent adsorption capacity [51]. The adsorption capacity and the presence of an electron shuttle are highly beneficial for the degradation of recalcitrant organic compounds in wastewater [52]. In addition, the proposed catalytic membrane allows for the degradation, separation, and microorganism retention in a single stage, thus intensifying the process.

Experimental

Membrane precursor preparation

Highly oxidised graphene powder (GO)

Highly oxidised graphene (GO) was synthesised following a modified Hummer's process [22]. Pristine graphite powder was purchased by Fluka with an average particle size of ≤20 μm. The starting material, i.e. graphite powder, was ground for 30 min by using mortar and pestle, and then 2.5 g of ground graphite was mixed with 2 g of $NaNO_3$ in a 250 ml flask. Sulphuric acid (70 ml) was added to the blend and stirred until homogenised. The mixture was cooled in an ice bath and 10 g of $KMnO_4$ was then added, and left overnight followed by heating at 50 °C for 24 h. Subsequently, 10 g of $KMnO_4$ and 70 ml of water were slowly added to the mixture and kept stirring for 24 h. The graphite oxide formed was poured into 400 ml of ice water, and then 3 ml of H_2O_2 was added and stirred overnight. The graphite oxide mixture was purified by dispersing in 500 ml aqueous solution of 3 wt% H_2SO_4 and 0.5 wt% H_2O_2. After 24 h, the graphite oxide pellet was collected by centrifuging at 3000 rpm for 30 min, and the supernatant was removed. This process was repeated five times. The solid product obtained was rinsed with copious water and dried in oven. Graphite oxide was exfoliated in water by ultrasonication for 2 h to obtain GO sheets. The GO dispersion was centrifuged at 1000 rpm for 5 min to remove thicker sheets, and the supernatant was again centrifuged at 3000 rpm for 30 min. The obtained GO pellet was dried in oven at 60 °C for 48 h. Before sonication and separation, the material is called graphite oxide, and after sonication and separation, the material is referred to as GO. All the chemicals were purchased from Sigma-Aldrich.

Nitrogen-doped reduced graphene oxide powder (NrGO)

The preparation of N-doped GO is based on previous studies showing that N-doped graphene exhibits better electrocatalytic activity than graphene [53]. The enhanced performance of N-graphene is mainly attributed to the existence of nitrogen functional groups, oxygen-containing groups and structural defects.

Nitrogen-doped reduced GO (NrGO) was synthesised through the solvothermal reaction of GO with ammonia and hydrazine [54]. In a typical experiment, synthesised GO was suspended in water to give a concentration of 1 mg ml^{-1} followed by sonication for 30 min to disperse the material in water. The pH of the solution was adjusted to 10 using ammonia hydroxide, and then 1 ml of hydrazine (35 wt% in H_2O) was added to the solution and stirred for 15 min. The resultant solution was transferred to a 100 ml Teflon-lined vessel to carry out the solvothermal reaction at 160 °C and 5 bar for 3 h. The resultant product was cleaned with plenty of deionised (DI) water and collected by centrifugation at 3000 rpm for 45 min. The pellet was dried under vacuum at 60 °C for 48 h.

Membrane supports

Composite ceramic discs (Ø47 mm; thickness 28 mm) made of TiO_2 with a slender superficial layer of ZrO_2–TiO_2 were provided by TAMI Industries (France); these are filtration elements in the range of ultrafiltration or fine ultrafiltration with different pore sizes equivalent to 1, 15, 50 and 150 kDa molecular weight cut-off (MWCO). Their intrinsic properties—physical strength, chemical and thermal

inertia or solvent insensitivity—make them suitable for synthesising membranes with relatively long-life and reusability after an adequate chemical cleaning procedure involving diluted nitric, phosphoric acid or sodium hydroxide. This fact is extremely beneficial with a view to a potential application in wastewater treatment or water purification.

Synthesis of graphene (GO or NrGO) membranes

Homogeneous GO or NrGO solutions were prepared by dispersing a certain amount (10 mg) of previously synthesised graphene powder into deionised water by sonication for 45 min. These solutions (GO or NrGO) were vacuum filtrated through the final membrane support, forming a superimposed film with controllable thickness on the surface of the ceramic support. The absence of requirement for peeling-off the deposited film reduces the preparation time. This length of time was around 5–15 min depending on the ceramic SPS. After the preparation, the membrane was dried for 24 h at 40 °C and ready to be used.

Membrane characterisation

Transmission electron microscopy (TEM JEOL, JEM-1011, USA) and environmental scanning electron microscopy (ESEM QUANTA 600, FEI, Dawson Creek Drive, Hillsboro, OR, USA) were used to study the synthesised material.

Membrane microstructure was examined by AFM (Pico Plus 2500 from Molecular Imaging, Bid-Service, LLC, Freehold, NJ, and USA), operating in the tapping mode.

Membrane precursor properties were further studied by conducting Raman spectroscopy. The analyses were performed at room temperature using a LabRAM 300 Raman spectrometer (Horiba Jobin–Yvon) equipped with a HeNe (633 nm) laser and a motorised XYZ mapping stage.

X-ray diffraction (XRD) measurements were also performed using a Bruker-AXS D8-discover diffractometer equipped with parallel incident beam (Göbel mirror), vertical θ–θ goniometer, XYZ motorised stage and a GADDS (General Area Diffraction System). Samples were placed directly on the sample holder, and the area of interest was selected with the aid of a video-laser focusing system. An X-ray collimator system allowed analysing areas of 500 μm. The X-ray diffractometer was operated at 40 kV and 20 mA, employing a monochromatic CuK_α radiation source ($\lambda = 1.54$ Å). The GADDS detector was a HI-STAR (multiwire proportional counter of 30 × 30 cm with a 1024 × 1024 pixel) placed at 15 cm from the sample and covering a range of 3°–37° 2θ.

The synthesised powders were also examined using an X-ray photoelectron spectroscopy (XPS) system (Kratos Axis Ultra DLD spectrometer) equipped with a monochromatic AlK_α X-ray (1486.6 eV). The chamber pressure was maintained below 2.39×10^{-11} bar, and surface charging was compensated with a secondary electron gun.

The membrane electrical resistance was measured using a multi-height microposition four-point probing system combined with a Keithley K2420 SourceMeter.

Membrane-filtration tests

The deionised (DI) water flux of the prepared membranes was measured in a dead-end cell (TAMI Industries) equipped to hold ceramic membranes in the form of discs. The effective area of membrane surface was 13.1 cm^2. All the experiments were carried out until reaching steady state of 25 °C and a constant transmembrane pressure of 0.2 bar. The permeate flux was continuously monitored by a precision balance and automatically recorded in a computer database. A scheme of the experimental setup is shown in Fig. 1.

Permeation flux is calculated according to the Eq. 1 [55].

$$J_w = \frac{V}{A \cdot t}, \tag{1}$$

where J_w is the pure water flux ($m^3\ m^{-2}\ h^{-1}$), V is the collected permeate volume (m^3), A is the membrane active area (m^2), and t is the permeation time (h).

Results and discussion

Graphene (GO or NrGO) synthesised powder characterisation

GO powder (1 mg) in N-methyl-2-pyrrolidone (NMP) solutions was characterised by ESEM and TEM (Figs. 2, 3) after applying ultrasounds for 15 min, followed by quick solvent evaporation using

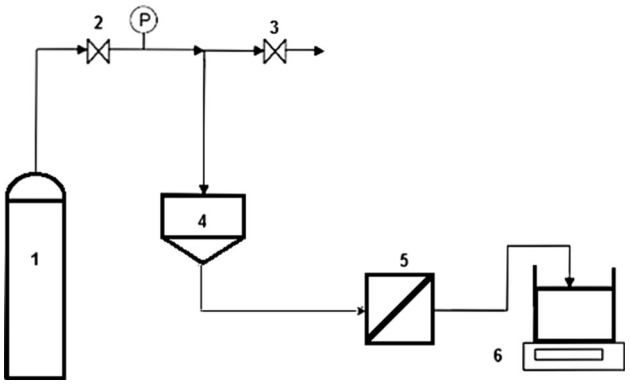

Figure 1 Dead-end filtration experimental setup: (*1*) nitrogen gas cylinder; (*2*) gas pressure regulator; (*3*) relief valve; (*4*) feed tank; (*5*) membrane holder; (*6*) weighing scale.

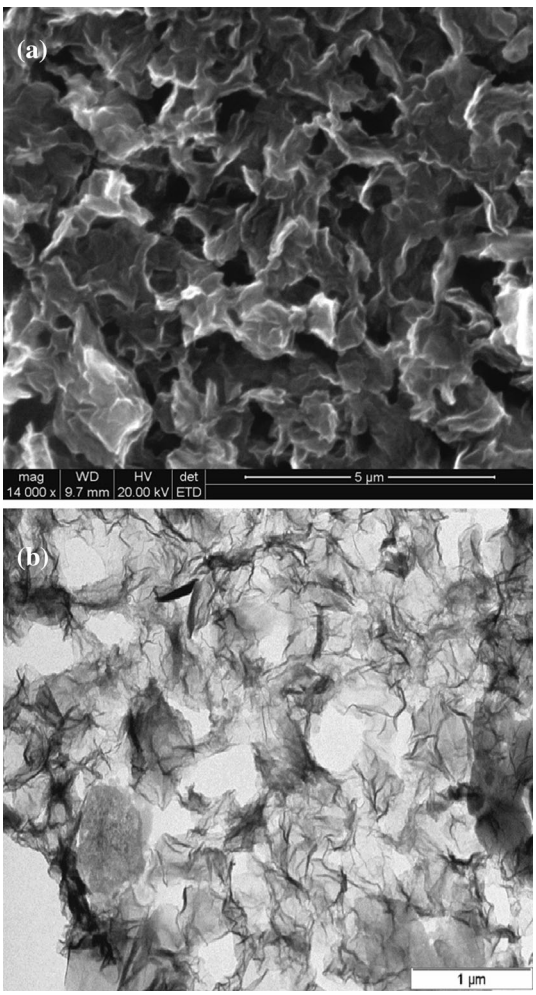

Figure 2 ESEM (**a**) and TEM (**b**) images of GO powder synthesised by a modification of Hummer's method. Hydrophilic GO powder (**a**, **b**) shows a 3D homogenous material distribution of particle aggregates.

infrared lamp. The powder sample was deposited onto an aluminium support, and the solvent was evaporated and immediately introduced into the ESEM. In the case of TEM analysis, a drop of sample was placed on a 200 µm mesh copper grid with a Formvar film.

On the other hand, NrGO sheets demonstrated a 3D wrinkled appearance of particle clusters with an interconnected porous network as observed elsewhere [22, 56]. Low-magnification TEM image (Fig. 3b) exhibited the same morphology, which is characteristic of NrGO powder produced by harsh oxidative and reductive treatments, and is indicative of defective structure.

The Raman spectra of GO and NrGO powders are shown in Fig. 4. The G and D bands in the case of GO are at 1584 and 1330 cm^{-1}. The G and D bands for NrGO are at 1574 and 1323 cm^{-1}, respectively. The shift in the G band position of NrGO towards lower wavelengths indicates decrease of the oxygen functional groups and recovery of sp^2 network following the solvothermal reduction. The I_D/I_G intensity ratio increased from 1.05 for GO to 1.4 for NrGO, suggesting the decrease in the size of sp^2 domains [54, 57]. It should be noted that in our study, an additional factor could be the incorporation of N dopants, which contributed to the enhancement of the D band intensity upon solvothermal reduction.

Figure 5 shows the XRD patterns of GO and NrGO powders. The XRD pattern of pristine graphite consists of a sharp peak at 26°, which corresponds to an interlayer spacing of 0.33 nm [58]. The complete absence of any peak at 2θ of 26° suggests that there are no graphitic contaminants present in the GO. Moreover, the GO pattern shows a characteristic peak at 11.9°, which corresponds to an interlayer distance of 0.7 nm. This indicates that the distance between the (002) planes of the graphite was increased due to the presence of high amount of oxygen functional groups produced through oxidation by the Hummer's method. After the solvothermal reduction with hydrazine, NrGO has two characteristic peaks at 2θ angles of 24° and 44°. The interlayer spacing of (002) plane of NrGO was calculated as 0.362 nm, which is greater than the atomic spacing of graphite (0.33 nm). This indicates that only a moderate level of oxidation is present in the NrGO.

X-ray photoelectron spectrometer (XPS) was used to determine the elemental compositions and bonding states of GO and NrGO. Figure 6a, b shows the C

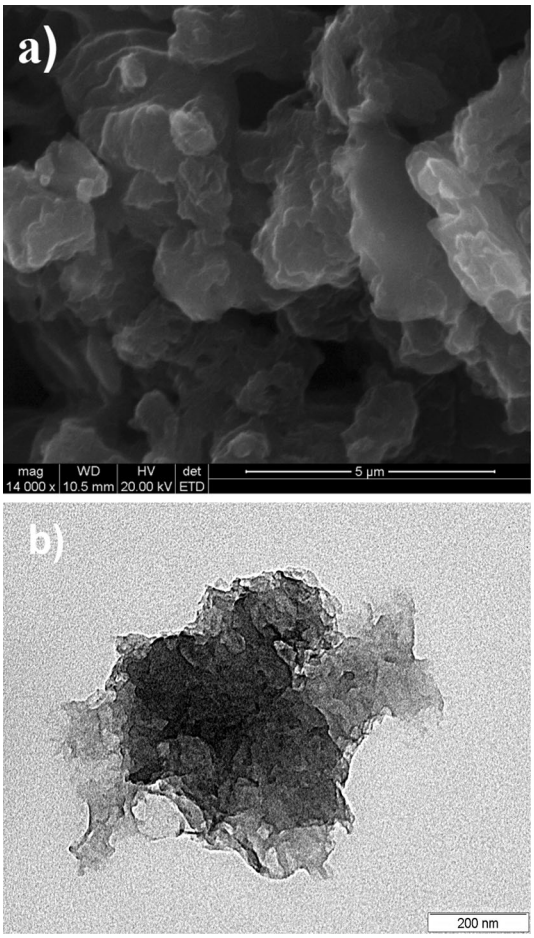

Figure 3 ESEM (**a**) and TEM (**b**) images of NrGO powder synthesised by solvothermal method.

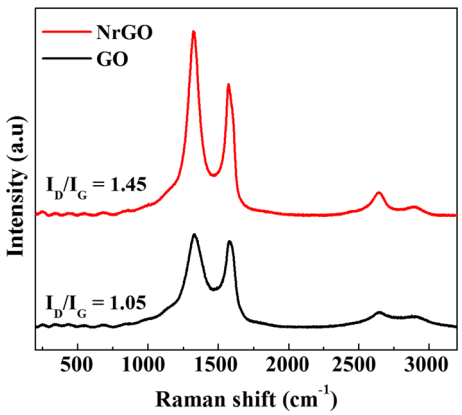

Figure 4 Raman spectrum of GO and NrGO powders.

1s of GO and NrGO. The high resolution C 1s of GO shows a well-defined peak at 286.46 eV, in addition to sp^2 carbon peak at 284.5 eV, which is a signature of extreme oxidation of GO. It can be noted that C 1s core-level spectra for GO contain four major peaks at 284.4, 285.1, 286.4 and 287.9 eV, which are attributed to the sp^2 carbon, hydroxyl (C–OH), epoxide (C–O–C) groups and the combined contribution from carbonyl (>C=O) and carboxyl (HO–C=O) groups, respectively [57]. The C 1s of NrGO can be fitted with three components at 284.4, 285.1 and 287.7 eV, which correspond to sp^2 carbon, C–N and also contributions from carbonyl and carboxylic groups [54].

Figure 6c shows the N 1s of NrGO, which can be considered being divided into four components: pyridinic N (398.8 eV), pyrrolic N (400.0 eV), graphitic N (401.54 eV), and pyridine N-oxide (403.4 eV), and these assignments are in agreement with the literature [59]. Figure 6d shows the elemental compositions of GO and NrGO. The C/O ratios in the case of GO and NrGO are 2.5 and 9.6, respectively, which show that oxygen content has been considerably reduced after solvothermal reduction with ammonia and hydrazine.

Membrane characterisation

Figure 7a, b shows membrane surfaces of the GO and NrGO, respectively, which evidences that homogeneous coating was performed since no significant defects were detected. However, in a potential application, the main role of the graphene would not only be catalysing the process, but also helping in the separation. In the specific case of GO membranes, the superficial layer adopted the same homogeneous porous structure as the conglomerate powder precursor (Figs. 2, 7c). On the contrary, the NrGO surface (Fig. 7d) exhibited a heterogeneous distribution in consonance with the powder precursor structure.

ESEM X-ray (EDX) system for chemical analysis was applied for the membrane surfaces of graphene (GO and NrGO)–ceramic, and the overall compositions are shown in Table 1.

It must be taken into account that the deposited GO is fragmented into particles or aggregates of different sizes, a fraction of them being small in size; therefore, they are probably able to penetrate into the ceramic support pores, thus conforming to a sort of composite (graphene–ceramic). Once the pores are constricted, on top of this composite, the GO sheets settle down and form a homogeneous GO layer. Therefore, the membrane is probably composed of a thin superficial layer of graphene (either GO or NrGO) followed by a

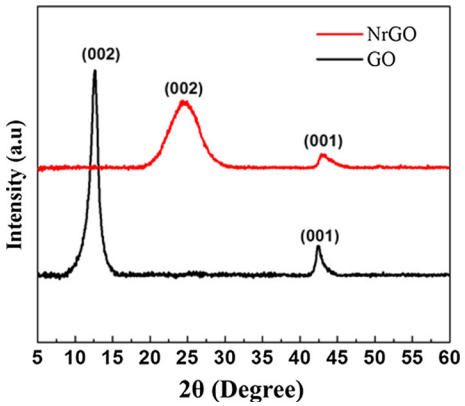

Figure 5 XRD characterisations of GO and NrGO powders.

composite of these compounds and ZrO_2, due to the graphene intrusion into the porous surface layer of the support, rich in ZrO_2. The membrane surface composition varied in both the cases. The use of reduced GO as membrane precursor increased the ratio C/O which is in concordance with the synthesised powder composition described in Fig. 6d. Note that the X-ray penetration depth under the operating conditions is estimated to be around 5 μm (20 kV), assuming the presence of only graphene (GO or NrGO). The detection of zirconia reduces this electron penetration depth to even lower values.

On the other hand, as can be seen in Fig. 7e, f, the GO and NrGO membrane thicknesses were about 7 and 9 μm, respectively.

The membrane surface was further investigated by AFM, and the height profiles are depicted in Fig. 8. A root-mean-square (RMS) roughness analysis was also applied to the membrane surface, as expected, and GO membrane showed much more roughness (136.1) than the NrGO ones (0.2). Both materials present a 3D multilayer structure. However, NrGO shows a less porous structure with punctual irregularities on its topography. GO membrane shows a porous structure with larger surface area, which could be interesting in specific applications where, besides the electrical conductivity, the adsorption plays an important role.

A rough estimation based on AFM imaging using SPIP™ software indicates that both membranes present most of the pores in the range of 20–40 nm.

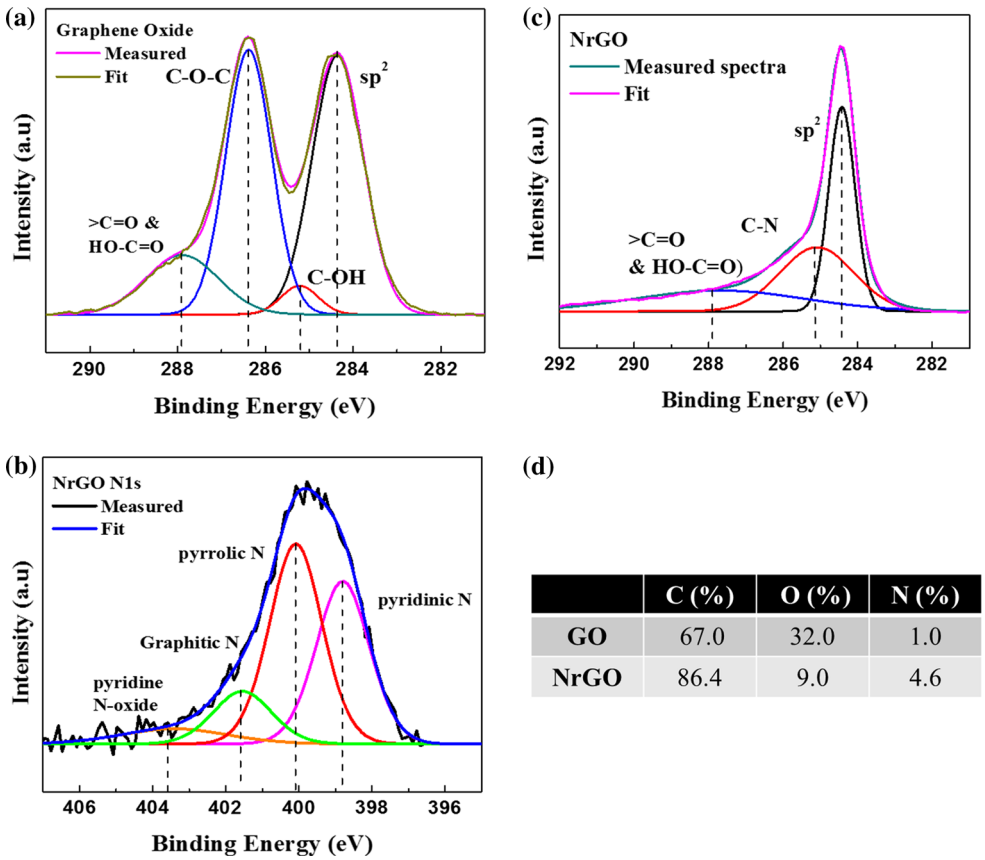

Figure 6 High-resolution C 1s XPS spectra of GO (**a**) and NrGO (**b**); high-resolution N 1s XPS spectra of NrGO (**c**); elemental composition of GO and NrGO (**d**).

(d)

	C (%)	O (%)	N (%)
GO	67.0	32.0	1.0
NrGO	86.4	9.0	4.6

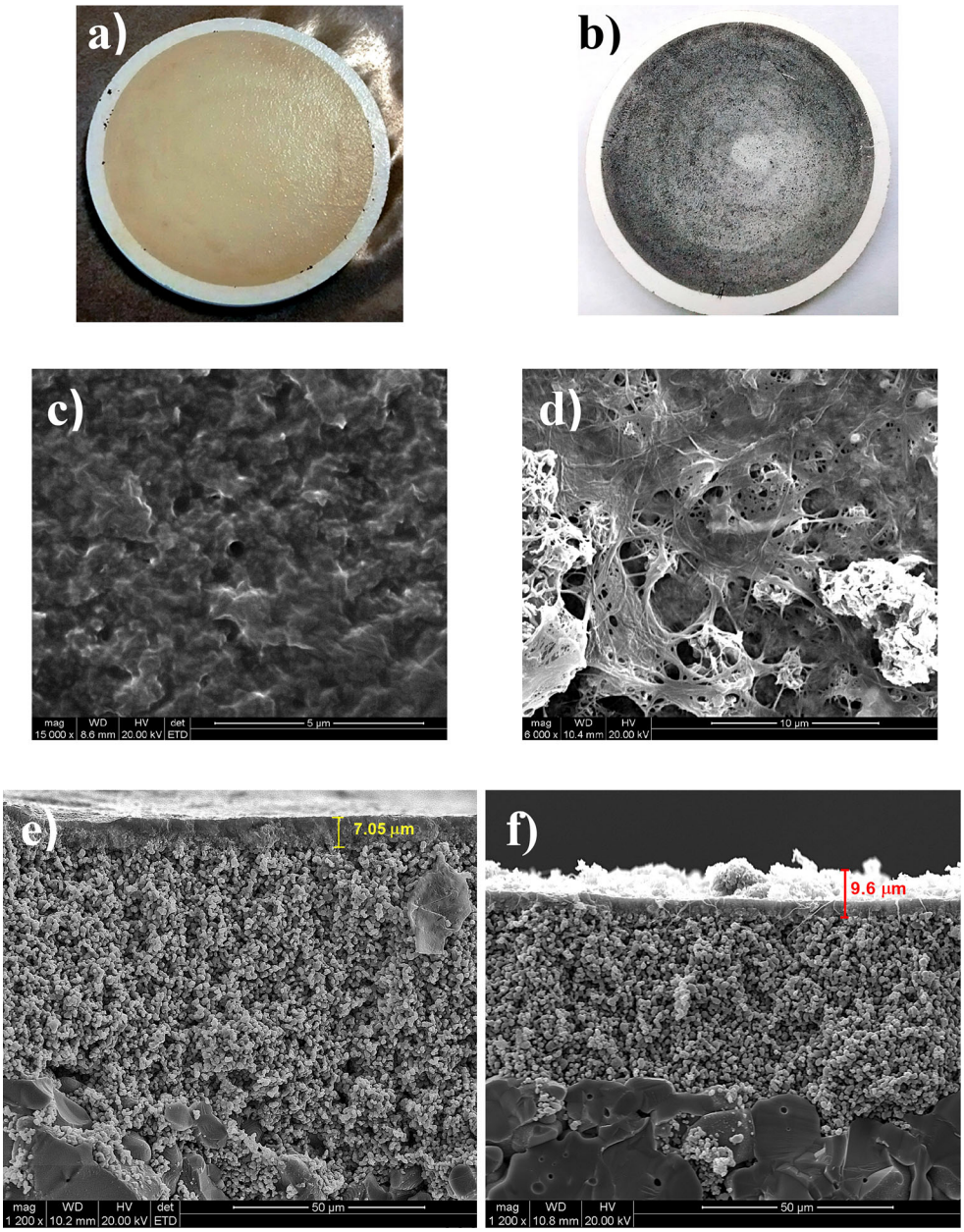

Figure 7 ESEM images: GO (**a**, **c**, **e**) and NrGO (**b**, **d**, **f**) discs, membrane surface, and cross-sectional view, respectively. (*ceramic support* 50 kDa; *deposited GO or NrGO amounts*: 0.1 mg).

Table 1 Elemental compositions of GO or NrGO composite membranes (wt%)

	C	O	Zr	Ti
GO	14.17	28.00	57.60	0.23
NrGO	33.48	23.49	41.73	1.30

Ceramic support 50 kDa, *deposited graphene amount* 0.1 mg

Nevertheless, the significant differences can be found on the areas occupied by these pores: 29.8 and 7.6 % for GO and NrGO membranes, respectively.

On the other hand, the electrical properties of the carbon membranes are a measure of its suitability in some wastewater processes such as photocatalytic degradation [60] and anaerobic biodegradation [50].

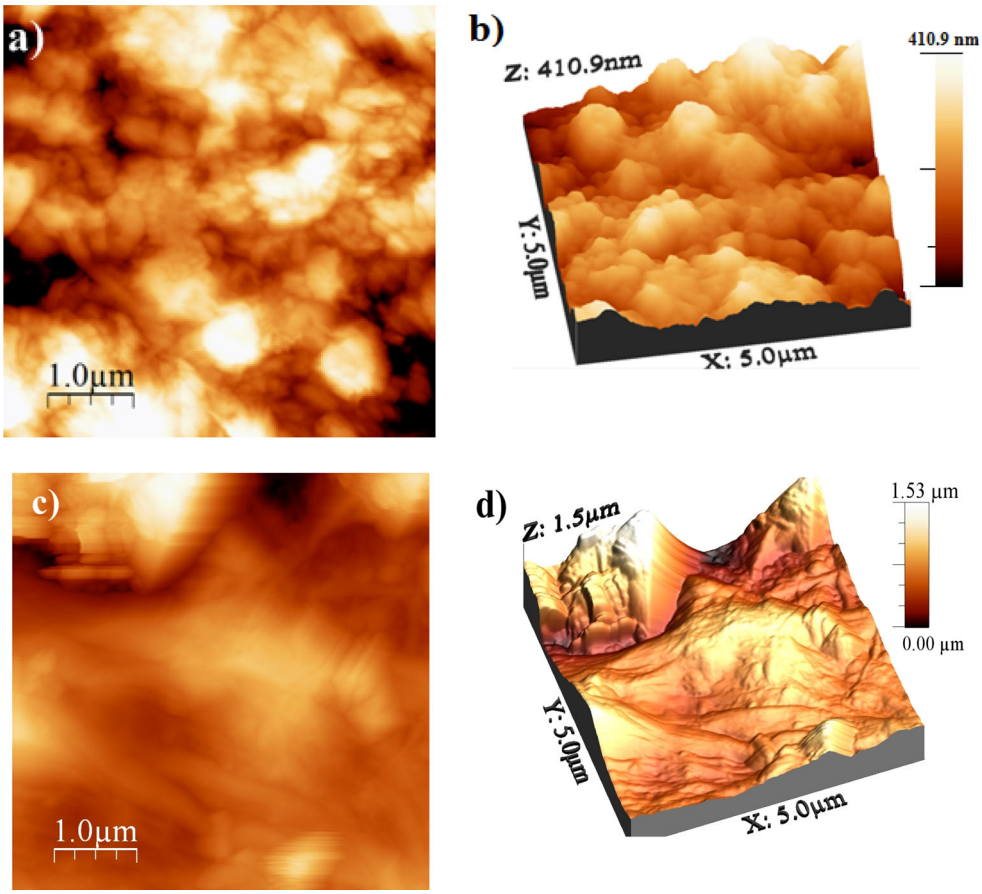

Figure 8 AFM images: GO (**a**, **b**) and NrGO (**c**, **d**) membrane topographies 2D, and 3D, respectively (*ceramic support* 50 kDa; *deposited GO or NrGO amount*: 0.1 mg).

The electrical resistance was measured using a multi-height microposition four-point probing system. On the contrary, the membrane thickness was defined by ESEM. Thus, the resistivity (Ω m) could be calculated using the Eq. 2:

$$\rho = R_s \cdot t, \tag{2}$$

where R_s (Ω) defines the electrical resistance, and t (m) corresponds to the sheet thickness. The calculated value for NrGO sheets was $\sim 2.8 \times 10^{-5}$ (Ω m) in agreement with previous studies [61]. This is more than 10–100 times lower than the resistances of similar sheets of amorphous carbon [62] typically used in such environmental applications.

Interactions on the membrane surface

Hydroxyl groups always exist on the surface of metal oxides such as ZrO_2 [60]; on the other hand, carboxyl groups are one of the main forms of oxygen-containing functions in oxidised graphene [63]. It has been reported that there is a significant attraction between hydroxyl and carboxyl groups [64]. For this reason, oxidised graphene would be partially ionised, creating anions and hydrogen cations, which would react with the hydroxyl groups on ZrO_2 surface. This phenomenon makes easier the synthesis of strong, continuous and homogeneous coatings over this type of ceramic materials. The interactions taking part in a similar process were already described by Hu et al. [40]. Although their study involved alumina modifications (AlO_2) with highly oxidised graphene, the mechanism could be assimilated in our study as illustrated in Fig. 9.

The use of reduced GO implies that a decrease in the presence of carboxyl groups weakens the interactions between both the materials. Thus, highly reduced GO may complicate the preparation of these composites.

Membrane permeation tests

DI water fluxes of the filtration element were measured before and after coating with GO or NrGO. Figure 10 plots the evolution of the water flux over the time.

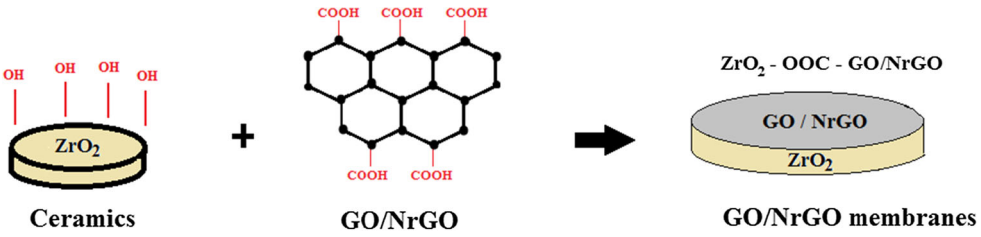

Figure 9 GO membrane over ZrO_2 surfaces. Interaction mechanism.

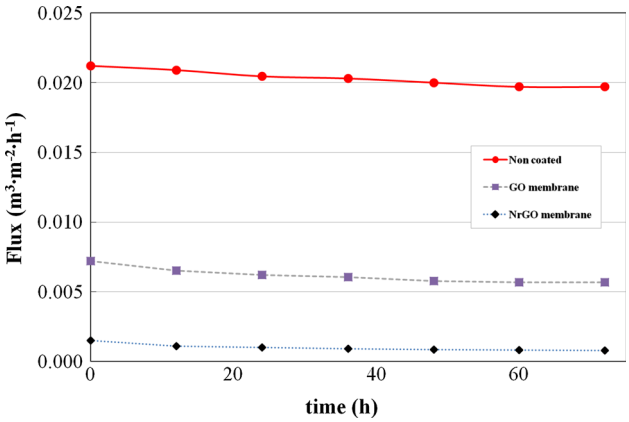

Figure 10 Pure water flux. (GO or NrGO deposited: 0.1 mg; ceramic support: 0.04 μm; hydraulic pressure difference: 0.2 bar).

As can be seen, the permeability decreases significantly due to the graphene layer deposition. Several empirical equations correlate permeability and membrane pore size. The Hagen–Poiseuille equation [65] is defined by Eq. 3:

$$J_w = \frac{\varepsilon \cdot r^2}{8 \cdot \mu \cdot \tau} \cdot \frac{\Delta P}{d}, \quad (3)$$

where ΔP is the hydraulic pressure difference (Pa), μ is the viscosity (Pa s), J_w is the pure water flux ($m^3\ m^{-2}\ s$), ε is the porosity, r is the pore radius (m), τ is the tortuosity and d is the membrane thickness (m).

Taking into account the Hagen–Poiseuille dependence and the experimental pure water flux reduction (71 %), the pore diameter in the GO membrane would be reduced by around 46 % with respect to the original size (assuming similar porosity, tortuosity and flux resistance controlled by the GO membrane). The pore constriction is usually associated with increase in the separation ability and lower permeations. However, in the case of high demanding fluxes, the pore size reduction can be limited by depositing smaller amounts of the membrane precursor. In addition, note that the filtration experiments were carried out at very low transmembrane pressures (0.2 bar), thus higher driving forces may be applied in case of specific requirements.

GO presents a 3D structure and relatively thick layers regarding graphene (2D) sheets. This fact not only has a clear detrimental impact on the permeation, but also increases the surface area, which is of great value in specific applications such as organic removal, e.g. photocatalytic degradation or anaerobic biodegradation, in wastewaters conducted over surface. The permeation was even lower for NrGO films probably due to its hydrophobic properties [66]. However, NrGO membranes offer less liquid permeation but higher electrical conductivity than GO layers do. Therefore, the selection of the proper membrane must be made depending on the requirements of a specific application.

In addition, potential applications such as water purification demand a stable performance for long periods. Tests conducted for 3 weeks showed that the flux was almost constant, which suggests no changes on membrane structure and guarantees their use for relatively long periods.

Some studies of GO membranes on alumina hollow fibre substrates reported drying-related shrinkage and instability at the dry state [41]. To check this effect, the disc membranes were subjected to drying for 24 h at 40 °C between two consecutives filtration tests. The experimental cycle was repeated twice in order to subject the membrane to further mechanical stress. Afterwards, no differences in permeability were found, thus refuting any drying-related problems. However, it must be noted that this phenomenon was indeed observed in case of depositing 1 mg or higher GO amounts (results not shown). In this case, membranes must be maintained in wet state in order to avoid any drying-related shrinkage and subsequent cracks.

Influence of membrane thickness

The impact of depositing different amounts of membrane precursor was studied. GO was chosen to carried out this investigation. The amount of GO deposited on the ceramic support can be easily

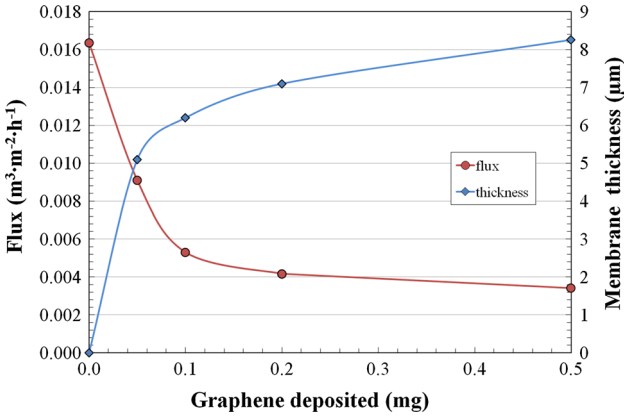

Figure 11 Dependence of the pure water flux on the GO deposited (ceramic support: 0.04 μm).

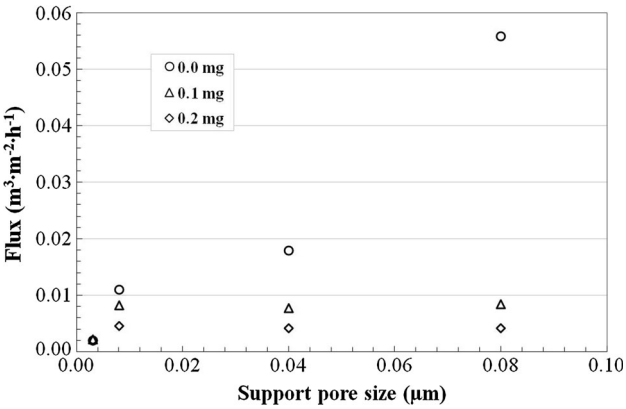

Figure 12 Influences of the support pore sizes on the permeate flux. (GO coated: 0.1 and 0.2 mg; hydraulic pressure difference: 0.2 bar; $T = 20$ °C).

controlled by using the vacuum filtration technique. The volume filtrated and corresponding GO concentration define the ultimate film thickness. As can be seen in Fig. 11, an increase of any of these variables provides thicker membranes.

In comparison to the ceramic support, the most important flux reduction (70 %) took place depositing small amounts (below 0.1 g) of GO. At this point, it is likely that the material filled completely the ceramic disc pores, and the pure water flux decreased notably from 0.017 to 0.005 $m^3\ m^{-2}\ h^{-1}$ (Fig. 11). For this reason, the deposition of larger amounts (0.5 g) of GO showed little additional impact on reducing the flux (4 %). Therefore, the graphene–ceramic composite zone exercises control over permeation, while superimposed GO layers impact the flux only slightly. This behaviour could be positive for specific applications where denser films of GO are needed.

In fact, the GO membrane physical structure as 3D aggregates and not 2D crystalline planes could be detrimental for filtration applications because of the additional membrane resistance and derived reduction on the permeation. However, GO membrane structure may benefit its performance in other processes where thicker and rougher films are preferable.

Support pore size influence on membrane preparation

The effect of the SPS in the preparation of highly oxidised graphene membranes was further studied. GO membranes were synthesised under identical conditions with the exception of the SPS. The permeability and membrane resistances, assuming a resistance in series model, are displayed in Fig. 12 and Table 2, respectively.

The overall membrane resistance R_m (m^{-1}) was calculated using the Eq. 4:

$$R_m = \sum R_i = R_s + R_{GO} = \frac{\Delta P}{\eta \cdot J_w}, \quad (4)$$

where R_s is the ceramic support resistance (m^{-1}), R_{GO} is the GO membrane resistance (m^{-1}), ΔP is the hydraulic pressure difference (Pa), J_w is the pure water flux ($m^3\ m^{-2}\ s^{-1}$), and η is the viscosity ($kg\ m^{-1}\ s^{-1}$).

As the resistance of the support, R_S, can be obtained from its original pure water flux, the additional resistance provided by the GO layer, R_{GO}, can be calculated.

Non-significant membrane resistance differences (≤10 %) were detected by modifying the SPS from 0.008 to 0.08 μm. As can be observed in Table 2, the pure water permeability was mostly governed by the GO layer intrinsic resistance independently of the SPS used. This can be explained by the ceramic disc pores constriction, which takes place in a greater or lesser extent depending on the initial pore size when the graphene sets down, yet reaching the same final state defined by the particles or aggregates deposited.

Note that the initial GO particles' aggregate size, which was estimated to be around 1 μm (Figs. 2, 3), changes after sonication and vacuum filtration due to the physical forces involved in these processes, and thus reaches smaller single particle or aggregate sizes allowing the penetration into the greater pores.

Table 2 Intrinsic GO layer and support resistances

SPS (μm)[a]	GO coated (mg)	$J \times 10^6$ ($m^3\ m^{-2}\ s^{-1}$)	$R_m \times 10^{-12}$ (m^{-1})	$R_s \times 10^{-12}$ (m^{-1})	$R_{GO} \times 10^{-12}$ (m^{-1})
0.003	0.0	0.6	34.7	34.7	0.0
0.003	0.1	0.4	47.3	34.7	12.6
0.003	0.2	0.3	59.5	34.7	24.8
0.008	0.0	3.1	6.5	6.5	0.0
0.008	0.1	2.3	8.7	6.5	2.2
0.008	0.2	1.3	15.8	6.5	9.3
0.040	0.0	5.0	4.0	4.0	0.0
0.040	0.1	2.2	9.3	4.0	5.3
0.040	0.2	1.2	17.2	4.0	13.2
0.080	0.0	15.5	1.3	1.3	0.0
0.080	0.1	2.4	8.5	1.3	7.2
0.080	0.2	1.2	17.2	1.3	15.9

Hydraulic pressure difference = 0.2 bar; T = 20 °C; *GO coated* 0.1 mg

[a] Estimated from the molecular weight cut-off (MWCO) by Crystal water manufacturer

On the contrary, the permeability of the ceramic support with the smallest pore size (0.003 μm) was only slightly diminished after depositing the carbon film. In this specific case, as can be observed in Table 2, the flux resistance is controlled by the ceramic support instead of the ultrathin GO layer. The most likely reason may be that the GO particles or aggregates settled onto the ceramic surface as they presented a bigger size than most ceramic pores (0.003 μm), so they were not able to penetrate the support pores. Therefore, the pore size was only slightly reduced, and its derived impact on the overall membrane resistance was less pronounced.

Conclusions

GO–ZrO_2 and NrGO–ZrO_2 membranes have been synthesised by means of the vacuum filtration technique. GO hydrophilicity favours the preparation of homogeneous precursor solutions and coatings. Moreover, the interactions between GO carboxyl and ceramic hydroxyl groups increase the robustness of these composites. In the specific case of NrGO–ZrO_2, although stable ultra-thin coatings were achieved, the coating was not as homogeneous as those derived from using GO powder because functional groups resulting from the chemical reduction of GO impart a hydrophobic character. These should be removed to improve the quality of these coatings.

GO–ZrO_2 membranes showed higher roughness than NrGO/ZrO_2. Their associated large surface area is required in specific applications where, besides the electrical conductivity, the adsorption plays an important role. On the other hand, NrGO membranes electroconductivity was found to be many orders of magnitude higher than that offered by other carbon forms such as GO or activated carbon. For this reason, these materials may enhance any water process such as photocatalytic decolourisation or anaerobic biodegradation of wastewaters where separation, surface area and electrical conductivity are simultaneously necessary.

In relation to the membrane synthesis, as expected, the precursor amount used determines the thickness. Thicker membranes provided lower permeability. However, note that the study is focused on composite membranes, and thus, the first GO layers deposited promoted the constriction of the support pores reducing its original flux to a greater extend. On the other hand, the SPS was changed in order to study the derived impact on the synthesised membrane. No differences were detected on the permeation that could be defined by the membrane precursor size.

Acknowledgements

The Spanish *Ministerio de Economía y Competitividad* is gratefully thanked for providing the financial

support through the Grants (CTM2011-23069 and CTM2015-67970) and funding the doctoral scholarship (BES-2012-059675). Some of the authors are recognised by the *Comissionat per a Universitats i Recerca del DIUE de la Generalitat de Catalunya* (2014 SGR 1065) and supported by the Universitat Rovira i Virgili (2014PFR-URV-B2-35). Support from the Department of Education and Learning (DEL) in Northern Ireland and the Ulster University in the form of two PhD studentships for JB and SKB is gratefully acknowledged.

References

[1] Novoselov KS, Geim AK, Morozov SV et al (2004) Electric field effect in atomically thin carbon films. Science 306:666–669. doi:10.1126/science.1102896

[2] Lee C, Wei X, Kysar JW, Hone J (2008) Measurement of the elastic properties and intrinsic strength of monolayer graphene. Science 321:385–388. doi:10.1126/science.1157996

[3] Ning J, Wang D, Zhang C et al (2015) Electrical and optical properties of layer-stacked graphene transparent electrodes using self-supporting transfer method. Synth Met 203:215–220. doi:10.1016/j.synthmet.2015.02.007

[4] Kang S-H, Fang T-H, Hong Z-H, Chuang C-H (2013) Mechanical properties of free-standing graphene oxide. Diam Relat Mater 38:73–78. doi:10.1016/j.diamond.2013.06.016

[5] Jagiello J, Judek J, Zdrojek M et al (2014) Production of graphene composite by direct graphite exfoliation with chitosan. Mater Chem Phys 148:507–511. doi:10.1016/j.matchemphys.2014.09.043

[6] Liu F, Seo TS (2010) Large scale synthetic method for free standing graphene film and graphene sponges. In: 10th IEEE Int. Conference Nanotechnol. IEEE, pp 696–699

[7] Campos-Delgado J, Botello-Méndez AR, Algara-Siller G et al (2013) CVD synthesis of mono- and few-layer graphene using alcohols at low hydrogen concentration and atmospheric pressure. Chem Phys Lett 584:142–146. doi:10.1016/j.cplett.2013.08.031

[8] Radchenko TM, Shylau AA, Zozoulenko IV (2014) Conductivity of epitaxial and CVD graphene with correlated line defects. Solid State Commun 195:88–94. doi:10.1016/j.ssc.2014.07.012

[9] Wu B, Tuncer HM, Katsounaros A et al (2014) Microwave absorption and radiation from large-area multilayer CVD graphene. Carbon 77:814–822. doi:10.1016/j.carbon.2014.05.086

[10] Grennberg H, Jansson U (2012) Advanced functional materials. Sci Technol Mol Condens Matter Biol Syst. doi:10.1016/B978-0-44-453681-5.00005-4

[11] Whitener KE, Sheehan PE (2014) Graphene synthesis. Diam Relat Mater 46:25–34. doi:10.1016/j.diamond.2014.04.006

[12] Potts JR, Dreyer DR, Bielawski CW, Ruoff RS (2011) Graphene-based polymer nanocomposites. Polymer (Guildf) 52:5–25. doi:10.1016/j.polymer.2010.11.042

[13] Zhao C, Xing L, Xiang J et al (2014) Formation of uniform reduced graphene oxide films on modified PET substrates using drop-casting method. Particuology 17:66–73. doi:10.1016/j.partic.2014.02.005

[14] William S, Hummers J, Offeman RE (1958) Preparation of graphitic oxide. J Am Chem Soc 80:1339. doi:10.1021/ja01539a017

[15] Nekahi A, Marashi PH, Haghshenas D (2014) Transparent conductive thin film of ultra large reduced graphene oxide monolayers. Appl Surf Sci 295:59–65. doi:10.1016/j.apsusc.2014.01.004

[16] Xu Y, Bai H, Lu G et al (2008) Flexible graphene films via the filtration of water-soluble noncovalent functionalized graphene sheets. J Am Chem Soc 130:5856–5857. doi:10.1021/ja800745y

[17] Chen C-M, Huang J-Q, Zhang Q et al (2012) Annealing a graphene oxide film to produce a free standing high conductive graphene film. Carbon 50:659–667. doi:10.1016/j.carbon.2011.09.022

[18] Noerochim L, Wang JZ, Wexler D et al (2013) Rapid synthesis of free-standing MoO_3/Graphene films by the microwave hydrothermal method as cathode for bendable lithium batteries. J Power Sources 228:198–205. doi:10.1016/j.jpowsour.2012.11.113

[19] Wei Z, Barlow DE, Sheehan PE (2008) The assembly of single-layer graphene oxide and graphene using molecular templates. Nano Lett 8:3141–3145. doi:10.1021/nl801301a

[20] Dolbin AV, Khlistyuck MV, Esel'son VB et al (2015) The effect of the thermal reduction temperature on the structure and sorption capacity of reduced graphene oxide materials. Appl Surf Sci. doi:10.1016/j.apsusc.2015.11.167

[21] Du X, Zhou C, Liu H-Y et al (2013) Facile chemical synthesis of nitrogen-doped graphene sheets and their electrochemical capacitance. J Power Sources 241:460–466. doi:10.1016/j.jpowsour.2013.04.138

[22] Bikkarolla SK, Papakonstantinou P (2015) $CuCo_2O_4$ nanoparticles on nitrogenated graphene as highly efficient oxygen evolution catalyst. J Power Sources 281:243–251. doi:10.1016/j.jpowsour.2015.01.192

[23] Li H, Song Z, Zhang X et al (2013) Ultrathin, molecular-sieving graphene oxide membranes for selective hydrogen separation. Science 342(80):95–98. doi:10.1126/science.1236686

[24] Liu R, Arabale G, Kim J et al (2014) Graphene oxide membrane for liquid phase organic molecular separation. Carbon 77:933–938. doi:10.1016/j.carbon.2014.06.007

[25] Li H, Song Z, Zhang X et al (2013) Ultrathin, molecular-sieving graphene oxide membranes for selective hydrogen separation. Science 342:95–98. doi:10.1126/science.1236686

[26] Eda G, Chhowalla M (2010) Chemically derived graphene oxide: towards large-area thin-film electronics and optoelectronics. Adv Mater 22:2392–2415. doi:10.1002/adma.200903689

[27] Paul DR (2012) Creating new types of carbon-based membranes. Sci 335:413–414. doi:10.1126/science.1216923

[28] Geim AK, Novoselov KSS (2007) The rise of graphene. Nat Mater 6:183–191. doi:10.1038/nmat1849

[29] Chen J, Guo Y, Huang L et al (2014) Controllable fabrication of ultrathin free-standing graphene films. Philos Trans R Soc A Math Phys Eng Sci 372:20130017. doi:10.1098/rsta.2013.0017

[30] Zheng Q, Li Z, Yang J, Kim J (2014) Graphene oxide-based transparent conductive films. Prog Mater Sci 64:200–247. doi:10.1016/j.pmatsci.2014.03.004

[31] Zheng Q, Shi L, Yang J (2012) Langmuir–Blodgett assembly of ultra-large graphene oxide films for transparent electrodes. Trans Nonferrous Met Soc China 22:2504–2511. doi:10.1016/S1003-6326(11)61492-1

[32] Xu Y, Long G, Huang L et al (2010) Polymer photovoltaic devices with transparent graphene electrodes produced by spin-casting. Carbon 48:3308–3311. doi:10.1016/j.carbon.2010.05.017

[33] Chowdhury S, Balasubramanian R (2014) Graphene/semiconductor nanocomposites (GSNs) for heterogeneous photocatalytic decolorization of wastewaters contaminated with synthetic dyes: a review. Appl Catal B 160–161:307–324. doi:10.1016/j.apcatb.2014.05.035

[34] Berdova M, Perros AP, Kim W et al (2014) Exceptionally strong and robust millimeter-scale graphene-alumina composite membranes. Nanotechnology 25:355701. doi:10.1088/0957-4484/25/35/355701

[35] Li N, Yang G, Sun Y et al (2015) Free-standing and transparent graphene membrane of polyhedron box-shaped basic building units directly grown using a NaCl template for flexible transparent and stretchable solid-state supercapacitors. Nano Lett 15:3195–3203. doi:10.1021/acs.nanolett.5b00364

[36] Feng X, Chen W, Yan L (2015) Free-standing dried foam films of graphene oxide for humidity sensing. Sensors Actuators B Chem 215:316–322. doi:10.1016/j.snb.2015.03.068

[37] Dikin DA, Stankovich S, Zimney EJ et al (2007) Preparation and characterization of graphene oxide paper. Nature 448:457–460. doi:10.1038/nature06016

[38] Rana K, Singh J, Lee JT et al (2014) Highly conductive freestanding graphene films as anode current collectors for flexible lithium-ion batteries. ACS Appl Mater Interfaces 6:11158–11166. doi:10.1021/am500996c

[39] Liu Y, Zhang D, Shang Y, Liu Y (2014) A simple route to prepare free-standing graphene thin film for high-performance flexible electrode materials. RSC Adv 4:30422. doi:10.1039/C4RA04031G

[40] Hu X, Yu Y, Zhou J et al (2015) The improved oil/water separation performance of graphene oxide modified $Al2O_3$ microfiltration membrane. J Memb Sci 476:200–204. doi:10.1016/j.memsci.2014.11.043

[41] Aba NFD, Chong JY, Wang B et al (2015) Graphene oxide membranes on ceramic hollow fibers—Microstructural stability and nanofiltration performance. J Memb Sci 484:87–94. doi:10.1016/j.memsci.2015.03.001

[42] Almandoz MC, Pagliero CL, Ochoa NA, Marchese J (2015) Composite ceramic membranes from natural aluminosilicates for microfiltration applications. Ceram Int 41:5621–5633. doi:10.1016/j.ceramint.2014.12.144

[43] Hatori H, Takagi H, Yamada Y (2004) Gas separation properties of molecular sieving carbon membranes with nanopore channels. Carbon 42:1169–1173

[44] Chen X, Dai Y, Wang X et al (2015) Synthesis and characterization of Ag_3PO_4 immobilized with graphene oxide (GO) for enhanced photocatalytic activity and stability over 2,4-dichlorophenol under visible light irradiation. J Hazard Mater 292:9–18. doi:10.1016/j.jhazmat.2015.01.032

[45] Kim H-S, Takizawa S, Ohgaki S (2007) Application of microfiltration systems coupled with powdered activated carbon to river water treatment. Wastewater Reclam Reuse Sustain 202:271–277. doi:10.1016/j.desal.2005.12.064

[46] Mezohegyi G, Bengoa C, Stuber F et al (2008) Novel bioreactor design for decolourisation of azo dye effluents. Chem Eng J 143:293–298

[47] Fu X, Yang H, Lu G et al (2015) Improved performance of surface functionalized TiO_2/activated carbon for adsorption–photocatalytic reduction of Cr(VI) in aqueous solution. Mater Sci Semicond Process 39:362–370. doi:10.1016/j.mssp.2015.05.034

[48] Chen J, Zhang F, Zhao Y-L et al (2016) Facile synthesis of CdS/C core–shell nanospheres with ultrathin carbon layer for enhanced photocatalytic properties and stability. Appl Surf Sci 362:126–131. doi:10.1016/j.apsusc.2015.11.197

[49] Fagan R, McCormack DE, Dionysiou DD, Pillai SC (2015) A review of solar and visible light active TiO2 photocatalysis for treating bacteria, cyanotoxins and contaminants of emerging concern. Mater Sci Semicond Process 42:2–14. doi:10.1016/j.mssp.2015.07.052

[50] Mezohegyi G, Gonçalves F, Órfão JJM et al (2010) Tailored activated carbons as catalysts in biodecolourisation of textile azo dyes. Appl Catal B 94:179–185. doi:10.1016/j.apcatb.2009.11.007

[51] Sun L, Yu H, Fugetsu B (2012) Graphene oxide adsorption enhanced by in situ reduction with sodium hydrosulfite to remove acridine orange from aqueous solution. J Hazard Mater 203–204:101–110. doi:10.1016/j.jhazmat.2011.11.097

[52] Mezohegyi G, van der Zee FP, Font J et al (2012) Towards advanced aqueous dye removal processes: a short review on the versatile role of activated carbon. J Environ Manag 102:148–164

[53] Shao Y, Zhang S, Engelhard MH et al (2010) Nitrogen-doped graphene and its electrochemical applications. J Mater Chem 20:7491. doi:10.1039/c0jm00782j

[54] Bikkarolla SK, Yu F, Zhou W et al (2014) A three-dimensional Mn_3O_4 network supported on a nitrogenated graphene electrocatalyst for efficient oxygen reduction reaction in alkaline media. J Mater Chem A 2:14493–14501. doi:10.1039/C4TA02279C

[55] Mobarakabad P, Moghadassi AR, Hosseini SM (2015) Fabrication and characterization of poly(phenylene ether-ether sulfone) based nanofiltration membranes modified by titanium dioxide nanoparticles for water desalination. Desalination 365:227–233. doi:10.1016/j.desal.2015.03.002

[56] Centeno A, Rocha VG, Alonso B et al (2013) Graphene for tough and electroconductive alumina ceramics. J Eur Ceram Soc 33:3201–3210. doi:10.1016/j.jeurceramsoc.2013.07.007

[57] Ganguly A, Sharma S, Papakonstantinou P, Hamilton J (2011) Probing the thermal deoxygenation of graphene oxide using high resolution in situ X-ray based spectroscopies. J Phys Chem C 115:17009–17019. doi:10.1021/jp203741y

[58] Bikkarolla SK, Cumpson P, Joseph P, Papakonstantinou P (2014) Oxygen reduction reaction by electrochemically reduced graphene oxide. Faraday Discuss 173:415–428. doi:10.1039/c4fd00088a

[59] Long D, Li W, Ling L et al (2010) Preparation of nitrogen-doped graphene sheets by a combined chemical and hydrothermal reduction of graphene oxide. Langmuir 26:16096–16102. doi:10.1021/la102425a

[60] Seven O, Dindar B, Aydemir S et al (2004) Solar photocatalytic disinfection of a group of bacteria and fungi aqueous suspensions with TiO2, ZnO and Sahara desert dust. J Photochem Photobiol A Chem 165:103–107. doi:10.1016/j.jphotochem.2004.03.005

[61] Pei S, Cheng HM (2012) The reduction of graphene oxide. Carbon 50:3210–3228. doi:10.1016/j.carbon.2011.11.010

[62] Ishak A, Rusop M (2014) Electrical Properties Of Intrinsic Amorphous Carbon Films From Ethanol Precursor. Int J Technol Enhanc Emerg Eng Res 3:305–308

[63] Oh YJ, Yoo JJ, Kim YI et al (2014) Oxygen functional groups and electrochemical capacitive behavior of incompletely reduced graphene oxides as a thin-film electrode of supercapacitor. Electrochim Acta 116:118–128. doi:10.1016/j.electacta.2013.11.040

[64] Wang L, Zhao J, Bai S et al (2014) Significant catalytic effects induced by the electronic interactions between carboxyl and hydroxyl group modified carbon nanotube supports and vanadium species for NO reduction with NH3 at low temperature. Chem Eng J 254:399–409. doi:10.1016/j.cej.2014.05.096

[65] Chen L, Feng H, Xie Z, Sun F (2014) "Disc-point" mass transfer Constructal optimizations with Darcy and Hagen–Poiseuille flows in porous media. Appl Math Model 38:1288–1299. doi:10.1016/j.apm.2013.08.015

[66] Fan L, Harris JL, Roddick FA, Booker NA (2001) Influence of the characteristics of natural organic matter on the fouling of microfiltration membranes. Water Res 35:4455–4463. doi:10.1016/S0043-1354(01)00183-X